

Title	Fabrication of CdSnP <sub>3</sub> Thin Films by Phosphidation for Photovoltaic Application
Author(s)	Nakatsuka, Shigeru; Inoue, Ryosuke; Nose, Yoshitaro
Citation	ACS Applied Energy Materials (2018), 1(4): 1635-1640
Issue Date	2018-04-23
URL	<a href="http://hdl.handle.net/2433/243851">http://hdl.handle.net/2433/243851</a>
Right	This document is the Accepted Manuscript version of a Published Work that appeared in final form in ACS Applied Energy Materials, copyright © American Chemical Society after peer review and technical editing by the publisher. To access the final edited and published work see <a href="https://doi.org/10.1021/acsaem.8b00079">https://doi.org/10.1021/acsaem.8b00079</a> .; This is not the published version. Please cite only the published version. この論文は出版社版ではありません。引用の際には出版社版をご確認ご利用ください。
Type	Journal Article
Textversion	author

# **Fabrication of CdSnP<sub>2</sub> Thin Films by Phosphidation for Photovoltaic Application**

Shigeru Nakatsuka\*, Ryosuke Inoue and Yoshitaro Nose

*Department of Materials Science and Engineering, Kyoto University, Kyoto 606-8501, Japan*

**Keywords:** II-IV-V<sub>2</sub>, chalcopyrite, CdSnP<sub>2</sub>, ZnSnP<sub>2</sub>, phosphidation

\* To whom all correspondence should be addressed. Tel.: +81-75-753-5472; Fax: +81-75-753-3579; E-mail: nakatsuka.shigeru.25c@kyoto-u.jp

## Abstract

We report on the fabrication of CdSnP<sub>2</sub> thin films for photovoltaic application. The phosphidation method, where co-sputtered Cd-Sn precursor thin film reacts with phosphorus gas, was utilized for the preparation of CdSnP<sub>2</sub> thin films. In order to establish the fabrication process, the temperature dependence on product phases was investigated and CdSnP<sub>2</sub> thin films were obtained by the phosphidation at 350 °C for 30 min under the phosphorus vapor pressure of 10<sup>-2</sup> atm. CdSnP<sub>2</sub> thin films showed a *n*-type conduction. The resistivity, the carrier concentration and the mobility were evaluated to be 3.5–3.7×10<sup>2</sup> Ω cm, 1–3×10<sup>15</sup> cm<sup>-3</sup> and 4.7–17 cm<sup>2</sup> V<sup>-1</sup> s<sup>-1</sup>, respectively. CdSnP<sub>2</sub> thin films with relatively flat and smooth surface were obtained, although it was reported that ZnSnP<sub>2</sub> with the same crystal structure grew as the protrusion shape by the VLS growth mode. In order to investigate these difference in growth mechanism between CdSnP<sub>2</sub> and ZnSnP<sub>2</sub>, the reaction process in Cd-Sn-P system was investigated and discussed based on the chemical potential diagrams. As the result, it was understood that Cd, Sn and P<sub>4</sub> directly reacted to form CdSnP<sub>2</sub>, while ZnSnP<sub>2</sub> was formed via the reaction among Zn<sub>3</sub>P<sub>2</sub>, Sn and P<sub>4</sub> after Zn reacts with P<sub>4</sub> to produce Zn<sub>3</sub>P<sub>2</sub>. Therefore, it is speculated that simple reaction route results in the high growth speed and smooth flat morphology was obtained in the fabrication of CdSnP<sub>2</sub> thin films.

## 1 **1. Introduction**

2 CuIn<sub>1-x</sub>Ga<sub>x</sub>Se<sub>2</sub> (CIGS) and CdTe are promising materials for thin film photovoltaic  
3 devices. The solar cells based on these chalcogenide compounds recorded the high  
4 conversion efficiencies of 22.6 %<sup>1</sup> for CIGS and 22.1 %<sup>2</sup> for CdTe, respectively. However,  
5 the usage of rare or toxic elements prevents the widespread use of these compound  
6 semiconductors. From these backgrounds, materials composed of non-toxic and earth-  
7 abundant elements have been researched and Cu<sub>2</sub>ZnSnS<sub>4-x</sub>Se<sub>x</sub> achieved the high  
8 conversion efficiency of 12.6 %.<sup>3</sup> In addition, Cu<sub>2</sub>SnS<sub>3</sub>,<sup>4</sup> Cu<sub>2</sub>O,<sup>5</sup> SnS,<sup>6</sup> FeS<sub>2</sub>,<sup>7</sup> and Zn<sub>3</sub>P<sub>2</sub><sup>8</sup>  
9 have been also investigated for the same concept.

10 ZnSnP<sub>2</sub> is also a promising material for solar absorber consisting of safe and earth-  
11 abundant elements. In the previous works, it was reported that ZnSnP<sub>2</sub> showed a *p*-type  
12 conduction with the carrier concentration of 10<sup>16</sup>–10<sup>18</sup> cm<sup>-3</sup> and a direct bandgap of ~ 1.6  
13 eV.<sup>9–16</sup> Based on Shockley-Queisser limit,<sup>17</sup> the theoretical conversion efficiency of about  
14 30% is calculated in the single-junction solar cell using ZnSnP<sub>2</sub> under the condition of  
15 AM 1.5 G solar spectrum.<sup>18</sup> The absorption coefficient of ZnSnP<sub>2</sub> was reported to be  
16 approximately 10<sup>5</sup> cm<sup>-1</sup> in visible light range,<sup>18,19</sup> which is comparable to that of  
17 CIGS.<sup>18,20</sup> Our research group reported that solar cells using ZnSnP<sub>2</sub> thin films<sup>21</sup> and bulk  
18 crystals<sup>15,22,23</sup>. The solar cells using ZnSnP<sub>2</sub> bulk crystals recorded the best conversion

1 efficiency of 3.44 % ( $J_{SC} = 12.3 \text{ mA/cm}^2$ ,  $V_{OC} = 0.472 \text{ V}$ ,  $FF = 0.594$ ).<sup>23</sup> The solar cell  
2 structure was Al/ZnO;Al/ZnO/(Cd,Zn)S/ZnSnP<sub>2</sub>/Cu. In this device, the value of  $V_{OC}$  was  
3 largely low considering the bandgap of ZnSnP<sub>2</sub>. XPS measurements revealed that  
4 CdS/ZnSnP<sub>2</sub> showed a large conduction band offset,  $\Delta E_C = -1.2 \text{ eV}$ ,<sup>24</sup> which suggested  
5 that band alignment was necessary to achieve a high conversion efficiency.

6 In this study, we focused on CdSnP<sub>2</sub> as a *n*-type material in the ZnSnP<sub>2</sub> solar cells.  
7 CdSnP<sub>2</sub> has a chalcopyrite structure as well as ZnSnP<sub>2</sub> and its bandgap is 1.17 eV.<sup>25</sup>  
8 Kumagai *et al.* carried out the first-principles calculation in ZnSnP<sub>2</sub> with chalcopyrite  
9 structure to obtain its band structure.<sup>26</sup> They reported that the valence band maximum  
10 (VBM) at the  $\Gamma$  point is mainly composed of P orbitals with slight hybridization with Zn  
11 and Sn orbitals and the conduction band minimum (CBM) is primarily composed of Zn  
12 and Sn cations orbitals. Consequently, the level of VBM in CdSnP<sub>2</sub> might be similar to  
13 that in ZnSnP<sub>2</sub> because of the same crystal structure and anions. This results in the  $\Delta E_C$   
14 value of  $-0.5 \text{ eV}$  between ZnSnP<sub>2</sub> and CdSnP<sub>2</sub> considering the difference of bandgap in  
15 both compounds and the improvement of band alignment is expected compared to CdS.  
16 In addition, it was reported that ZnSnP<sub>2</sub> and CdSnP<sub>2</sub> form a solid solution in all  
17 composition range,<sup>27</sup> which suggests the intermixing of Zn and Cd atoms at  
18 CdSnP<sub>2</sub>/ZnSnP<sub>2</sub> interface and *pn*-junction with few band offset and interfacial defect can

1 be formed. However, few reports on the formation of CdSnP<sub>2</sub> thin films are available.

2 In this report, we thus tried to establish the fabrication process to obtain CdSnP<sub>2</sub> thin  
3 films, where Cd-Sn precursor thin films react with phosphorus gas, so-called  
4 phosphidation. Particularly, the impact of reaction temperature on product phases was  
5 investigated and morphology change was discussed based on the chemical potential  
6 diagrams.

## 7 **2. Experimental method**

8 Cd-Sn thin films with the thickness of 0.5 μm were fabricated as a precursor on soda  
9 lime glass substrates by magnetron direct current sputtering with a base pressure of  
10  $5 \times 10^{-4}$  Pa. The 1 inch target materials of Cd (99.9 %, Kojundo Chemical Laboratory) and  
11 Sn (99.99%, Furuuchi Chemical) were co-sputtered for 45 min under an Ar atmosphere  
12 with the pressure of 0.8 Pa and the gas flow rate of 20 sccm. The power densities for Cd  
13 and Sn targets were set at 0.6 and 3.2 W/cm<sup>2</sup>, respectively. During the sputtering, the  
14 substrates were rotated at 12 rpm without heating. For the safety sputtering of Cd, the  
15 target materials were sufficiently cooled down for more than 30 min. Dust collecting  
16 should be utilized when sample are extracted from a sputtering chamber. The thickness  
17 and composition were measured by inductively coupled plasma-atomic emission  
18 spectroscopy (ICP-AES, SII Nano Technology SPS3520UV). The samples were

1 dissolved in inverse aqua regia ( $\text{HNO}_3:\text{HCl} = 3:1$ ) and the solution 1/10~~0~~-diluted with  
2 deionized water was used for the ICP-AES measurements. Considering the higher vapor  
3 pressure of Cd, the molar ratio  $[\text{Cd}]/[\text{Sn}]$  was controlled to be about 1.2 in the precursor  
4 thin films.

5 Then, Cd-Sn thin films reacted with phosphorus gas to obtain  $\text{CdSnP}_2$  thin films by  
6 phosphidation. The details of the experimental conditions were described in our previous  
7 work.<sup>28</sup> We used two phase sample with Sn and  $\text{Sn}_4\text{P}_3$  as a phosphorus source and  
8 phosphorus gas was transported to the precursor thin films using Ar carrier gas, which  
9 was deoxidized by passing through a Ti sponge heated at 900 °C. The partial pressure of  
10 phosphorus was set at approximately  $10^{-2}$  atm by controlling the temperature of two phase  
11 sample. In this study, the phosphidation temperatures were 300, 350 and 400 °C. After  
12 the phosphidation, the thin films were cooled down in the furnace by turning off the heater,  
13 or quenched outside the furnace. The surficial and cross-sectional morphology of thin  
14 films before and after phosphidation were analysed by scanning electron microscopy  
15 (SEM, HITACHI S-3500H and HITACHI SU-1500) The product phases were identified  
16 by X-ray diffraction (XRD, Panalytical X'Pert Pro Alpha-1), where  $\text{CuK}\alpha_1$  ( $\lambda=1.5406$   
17 Å) was used as an incident X-ray (45 kV, 40 mA) in Bragg–Brentano ( $\theta$ – $2\theta$ ) configuration.  
18 **In order to evaluate the electrical properties, Hall effect and resistivity measurements**

1 were carried out at room temperature based on van der Pauw method using Hall-resistivity  
2 measurement system (Toyo Technica, ResiTest8300).

3 For the consideration of growth mechanism in the phosphidation method, we used the  
4 chemical potential diagrams. The review on the chemical potential diagrams is well  
5 summarized by Yokokawa.<sup>29</sup> A chemical potential diagram shows a stable potential  
6 region in various substances and each axis represents a chemical potentials of constituent  
7 elements. The chemical potential diagram of the Cd-Sn-P system was drawn using the  
8 software, Chesta 3.2.6.9, developed by Hatada. In order to obtain the potential diagrams,  
9 the thermodynamic data for Cd (g) and Sn (g) were derived from the database edited by  
10 Barin<sup>30</sup>. The Gibbs energies of formation for CdP<sub>2</sub> (s), Cd<sub>3</sub>P<sub>2</sub> (s) and CdSnP<sub>2</sub> (s) reported  
11 by Sirota *et al.*<sup>31</sup> and Smolyarenko *et al.*<sup>32</sup> were also utilized.

## 12 **3. Results and discussion**

### 13 **3.1. Effect of phosphidation temperature**

14 In order to obtain CdSnP<sub>2</sub> thin films with the single-phase, the phosphidation of Cd-Sn  
15 precursor thin films was carried out at various reaction temperatures such as 300, 350 and  
16 400 °C. In each experiment, Cd-Sn precursor thin films reacted with phosphorus gas for  
17 30 min and then was cooled down in the furnace. Figure 1 shows the XRD profiles of Cd-  
18 Sn precursor thin films before and after phosphidation. In the precursor thin film, Cd and



1 Sn were identified and alloy was not observed, because Cd-Sn system is a typical eutectic  
2 system. The formation of  $\text{CdSnP}_2$  as a main phase was observed in the phosphidation at  
3 300 and 350 °C. In particular, all reflections observed in the sample prepared at 350 °C  
4 were corresponded to the reflections of  $\text{CdSnP}_2$ . In addition, those samples show (112)  
5 plane orientation of  $\text{CdSnP}_2$ , which is a close-packed plane in chalcopyrite structure. ICP-  
6 AES analysis showed that the composition of the thin film fabricated at 350 °C was 27.2  
7 at. % Cd, 23.6 at. % Sn and 53.2 at.% P, which is Cd-rich composition compared with the  
8 stoichiometric ratio of  $\text{CdSnP}_2$ . In some samples prepared by the same condition,  $\text{Cd}_3\text{P}_2$   
9 was identified from XRD profiles. Therefore, the existence of  $\text{Cd}_3\text{P}_2$  as a secondary phase  
10 is considered even in the case that  $\text{Cd}_3\text{P}_2$  is not identified in XRD profiles as shown in  
11 Fig. 1. While,  $\text{Cd}_6\text{P}_7$  and Sn were identified in addition to  $\text{CdSnP}_2$  in the sample for 400  
12 °C.

13 Figure 2 shows SEM images of Cd-Sn precursor thin films before and after  
14 phosphidation. The Cd-Sn precursor thin film was composed of sub-micron particles. On  
15 the other hand, the sub-micron particles were not observed in the thin film after  
16 phosphidation at 300 °C, which was the morphology indicating that metal precursor  
17 melted. The phosphidation at 350 °C resulted in the  $\text{CdSnP}_2$  thin film consisting of  
18 particles with the diameter of about 1  $\mu\text{m}$ . The particles with the diameter of a few  $\mu\text{m}$

1 were formed on the surface of the thin film in the sample after phosphidation at 400 °C.  
2 Such particles might be secondary phases containing Sn. The cross-sectional SEM  
3 observation was carried out in Cd-Sn precursor thin film and CdSnP<sub>2</sub> thin film fabricated  
4 by the phosphidation at 350 °C as shown in Fig. 3. In the Cd-Sn precursor thin film, it is  
5 observed that sub-micron particles were deposited on the glass substrate, while CdSnP<sub>2</sub>  
6 film shows the dense microstructure consisting of granular particles compared with the  
7 Cd-Sn precursor thin film. This implies that phosphidation reaction proceeded as metal  
8 precursor partly-melted. In addition, it is confirmed that the thickness of the film was  
9 reduced, which might be attributed to the evaporation of precursor metal. ICP-AES  
10 analysis also clarified that a half amount of precursor metal, Cd and Sn, evaporated during  
11 the phosphidation experiments at 350 °C, which has to be improved in future work. The  
12 Hall measurement indicates that CdSnP<sub>2</sub> thin films prepared by the phosphidation has the  
13 *n*-type conduction as well as the CdSnP<sub>2</sub> bulk crystals grown by the solution method.<sup>25</sup>  
14 CdSnP<sub>2</sub> thin films showed a *n*-type conduction. The resistivity, the carrier concentration  
15 and the mobility were evaluated to be  $3.5\text{--}3.7\times 10^2 \Omega \text{ cm}$ ,  $1\text{--}3\times 10^{15} \text{ cm}^{-3}$  and  $4.7\text{--}17 \text{ cm}^2$   
16  $\text{V}^{-1} \text{ s}^{-1}$ , respectively.

17 As mentioned above, CdSnP<sub>2</sub> thin films were obtained by the phosphidation of Cd-Sn  
18 precursor thin films at 350 °C for 30 min. In addition, CdSnP<sub>2</sub> thin films has relatively

1 smooth morphology compared with ZnSnP<sub>2</sub> thin films. In our previous work, a different  
2 surface morphology was observed in ZnSnP<sub>2</sub> thin films fabricated even by a similar  
3 phosphidation process.<sup>28</sup> Some ZnSnP<sub>2</sub> protrusions with the length of a few μm were  
4 formed on the ZnSnP<sub>2</sub> thin film by so-called VLS (Vapor-Liquid-Solid) growth mode.<sup>28,33</sup>  
5 It is interesting that CdSnP<sub>2</sub> and ZnSnP<sub>2</sub> showed different morphologies in spite of the  
6 similarity in constituent elements and crystal structures.

### 7 **3.2. Growth mechanism of CdSnP<sub>2</sub> thin film**

8 The time dependence of phosphidation in CdSnP<sub>2</sub> was investigated in order to clarify  
9 the growth mechanism. Here, we prepared a sample discontinued at 250 °C on the way  
10 heating up to 300 °C and another one after the phosphidation of Cd-Sn thin film at 300  
11 °C for 2 min. Each sample was quenched outside the furnace in order to freeze the state  
12 during the phosphidation, while samples as shown in the previous section were  
13 conventionally cooled in the furnace after phosphidation. Figure 4 shows the XRD profile  
14 for each sample. The discontinued sample indicates that phosphidation reaction had not  
15 started at the heating stage because precursor metals such as Cd and Sn were identified.  
16 On the other hand, CdSnP<sub>2</sub> is observed as a main phase even in the phosphidation for 2  
17 min, which suggests that the reaction rate to form CdSnP<sub>2</sub> is higher compared with  
18 ZnSnP<sub>2</sub> fabricated by the same phosphidation method. In the case of ZnSnP<sub>2</sub>, 5 min

1 phosphidation did not finish the formation of  $\text{ZnSnP}_2$  even in the higher reaction  
2 temperature of 450 °C. It is also understood that partly-melted precursor metal is an  
3 important factor for fast phosphidation reaction from the SEM images of the film surface  
4 shown in Figure 5, as previously predicted.

5 Here, the difference of the surface morphologies between  $\text{CdSnP}_2$  and  $\text{ZnSnP}_2$  films is  
6 discussed. In this study, we consider the difference in growth mechanism between both  
7 based on the chemical potential diagrams, because the morphology might depend on the  
8 growth mechanism of each thin film. Figure 6 shows the chemical potential diagrams of  
9 the Cd-Sn-P system at 300 °C together with the diagram of the Zn-Sn-P system at 450 °C,  
10 which was previously reported by our group.<sup>28</sup> The logarithms of the partial pressures of  
11 Cd (g), Zn (g), Sn (g) and  $\text{P}_4$  (g) were used as the axes, which represent their chemical  
12 potentials. The dotted line indicates the partial pressure of  $\text{P}_4$  (g) controlled in the  
13 experiments:  $10^{-2}$  atm.

14 We discuss the phosphidation process of Cd-Sn precursor thin films as well as the case  
15 of Zn-Sn films. The point A in Figure 6a represents the state for Cd-Sn precursor thin  
16 films before phosphidation. Then, the chemical potential of phosphorus in the film  
17 increases with keeping the equilibrium of Cd (l) and Sn (l) as the phosphidation reaction  
18 proceeds, and at the point B,  $\text{CdSnP}_2$  (s) forms. On the other hand, in the Zn-Sn-P system

1 shown in Figure 6b, the phosphorus potential for the formation of  $\text{ZnSnP}_2$  (s) shown by  
2 point D is much higher than that for  $\text{Zn}_3\text{P}_2$  (s) shown by point C. It is thus understood that  
3 the formation of  $\text{Zn}_3\text{P}_2$  (s) preferentially occurs before  $\text{ZnSnP}_2$  (s) in the Zn-Sn-P system.  
4 Such a behaviour was experimentally observed in our previous work.<sup>28</sup> The previous  
5 work also showed that the surface morphology of  $\text{ZnSnP}_2$  thin films was rough and some  
6 protrusions were grown. To discuss the roughness of  $\text{ZnSnP}_2$  thin films, two issues during  
7 phosphidation should be considered. One is the microstructure of the Zn-Sn precursor  
8 thin films before phosphidation, where it was observed that the separation of Zn and Sn  
9 grains and the cohesion of Sn with the grain size of a few micron. The separation is  
10 expected from the phase diagram of the Zn-Sn system. The other one is a phosphidation  
11 process, which was investigated experimentally and thermodynamically. The formation  
12 of  $\text{ZnSnP}_2$  protrusions by VLS growth mode is due to the above two issues. On the other  
13 hand, the grain size in Cd-Sn precursor thin films is sub-micron as shown in Figure 2a  
14 although the separation of Cd and Sn is observed. In addition, the equilibrium chemical  
15 potential of phosphorus with  $\text{CdSnP}_2$  is lower than that with  $\text{Cd}_3\text{P}_2$  as shown in Figure 6a,  
16 which suggests that  $\text{CdSnP}_2$  forms without the formation of other phases as described  
17 above. These are different with the case of  $\text{ZnSnP}_2$ , and key conditions to obtain a smooth  
18 surface of  $\text{CdSnP}_2$  films.

## 1 4. Conclusions

2 In this study, we investigated the temperature dependence in phosphidation of Cd-Sn thin  
3 films on product phases and CdSnP<sub>2</sub> thin films were prepared at 350 °C for 30 min under  
4 the phosphorus vapor pressure of 10<sup>-2</sup> atm. CdSnP<sub>2</sub> thin films showed a *n*-type conduction.  
5 CdSnP<sub>2</sub> thin films showed a *n*-type conduction. The resistivity, the carrier concentration  
6 and the mobility were evaluated to be 3.5–3.7×10<sup>2</sup> Ω cm, 1–3×10<sup>15</sup> cm<sup>-3</sup> and 4.7–17 cm<sup>2</sup>  
7 V<sup>-1</sup> s<sup>-1</sup>, respectively. The SEM observation suggested that CdSnP<sub>2</sub> thin films with  
8 relatively flat and smooth surface were obtained, although the formation of ZnSnP<sub>2</sub>  
9 protrusions by the VLS growth mode was reported in the case of the Zn-Sn-P system. In  
10 order to investigate the difference in both systems, the reaction process in the Cd-Sn-P  
11 system was investigated and discussed based on the chemical potential diagrams. The  
12 experimental results and the chemical potential diagram suggested that Cd, Sn and P<sub>4</sub>  
13 directly reacted to form CdSnP<sub>2</sub>, while ZnSnP<sub>2</sub> was formed via the reaction among Zn<sub>3</sub>P<sub>2</sub>,  
14 Sn and P<sub>4</sub> after Zn reacts with P<sub>4</sub> to produce Zn<sub>3</sub>P<sub>2</sub>. Therefore, it is concluded that direct  
15 reaction route to form CdSnP<sub>2</sub> results in the high growth rate and flat morphology in the  
16 fabrication of CdSnP<sub>2</sub> thin films.

## 1 **Acknowledgements**

- 2 The authors wish to thank Assistant Prof. N. Hatada (Kyoto Univ.) for the provision of  
3 Chesta, software for creating chemical potential diagrams. This work was financially  
4 supported by JST CREST Grant Number JPMJCR17J2, The Mitsubishi Foundation and  
5 Grant-in-Aid for JSPS Research Fellow Number 16J09443.

## References

- (1) Jackson, P.; Wuerz, R.; Hariskos, D.; Lotter, E.; Witte, W.; Powalla, M. Effects of Heavy Alkali Elements in Cu(In,Ga)Se<sub>2</sub> Solar Cells with Efficiencies up to 22.6%. *Phys. Status Solidi RRL* **2016**, *10*, 583-586.
- (2) First Solar. First Solar Hits Record 22.1% Conversion Efficiency for CdTe Solar Cell. <https://www.greentechmedia.com/articles/read/First-Solar-Hits-Record-22.1-Conversion-Efficiency-For-CdTe-Solar-Cell> (last accessed January 2018).
- (3) Wang, W.; Winkler, M. T.; Gunawan, O.; Gokmen, T.; Todorov, T. K.; Zhu, Y.; Mitzi, D. B. Device Characteristics of CZTSSe Thin-Film Solar Cells with 12.6% Efficiency. *Adv. Energy Mater.* **2014**, *4*, 1301465.
- (4) Nakashima, M.; Fujimoto, J.; Yamaguchi, T.; Izaki, M. Cu<sub>2</sub>SnS<sub>3</sub> Thin-Film Solar Cells Fabricated by Sulfurization from NaF/Cu/Sn Stacked Precursor. *Appl. Phys. Express* **2015**, *8*, 42303.
- (5) Minami, T.; Nishi, Y.; Miyata, T. Heterojunction Solar Cell with 6% Efficiency Based on an N-Type Aluminum-Galium-Oxide Thin Film and P-Type Sodium-Doped Cu<sub>2</sub>O Sheet. *Appl. Phys. Express* **2015**, *8*, 22301.
- (6) Sinsersuksakul, P.; Sun, L.; Lee, S. W.; Park, H. H.; Kim, S. B.; Yang, C.; Gordon, R. G. Overcoming Efficiency Limitations of Sn-S-Based Solar Cells. *Adv.*



*Energy Mater.* **2014**, *4*, 1400496.

- (7) Ennaoui, A.; Tributsch, H. Iron Sulphide Solar Cell. *Sol. Cells* **1984**, *13*, 197-200.
- (8) Bhushan, M.; Catalano, A. Polycrystalline Zn<sub>3</sub>P<sub>2</sub> Schottky Barrier Solar Cells. *ppl. Phys. Lett.* **1981**, *38*, 39-41.
- (9) Abdurakhimov, A. A.; Kradinova, L. V.; Parimbekov, Z. A.; Rud' , Y. V. chottky Diodes Made of P-Type ZnSnP<sub>2</sub>. *Sov. Phys. Semicond.* **1982**, *16*, 156-59.
- (10) Ryan, M. A.; Peterson, M. W.; Williamson, D. L.; Frey, J. S.; Maciel, G. E.; arkinson, B. A. Metal Site Disorder in Zinc Tin Phosphide. *J. Mater. Res.* **1987**, , 528-537.
- (11) Nakatsuka, S.; Nakamoto, H.; Nose, Y.; Uda, T.; Shirai, Y. Bulk Crystal Growth and Characterization of ZnSnP<sub>2</sub> Compound Semiconductor by Flux Method. *Phys. Status Solidi C* **2015**, *12*, 520-523.
- (12) Scanlon, D. O.; Walsh, A. Bandgap Engineering of ZnSnP<sub>2</sub> for High-Efficiency Solar Cells. *Appl. Phys. Lett.* **2012**, *100*, 251911.
- (13) Hinuma, Y.; Oba, F.; Nose, Y.; Tanaka, I. First-Principles Study of Valence Band Offset at ZnSnP<sub>2</sub>/CdS, ZnSnP<sub>2</sub>/ZnS, and Related Chalcopyrite/Zincblende Heterointerfaces. *J. Appl. Phys.* **2013**, *114*, 043718.
- (14) Ajmera, P. K.; Shin, H. Y.; Zamanian, B. Vacuum Growth of Thin Films of ZnSnP<sub>2</sub>.

- Sol. Cells* **1987**, *21*, 291-299.
- (15) Nakatsuka, S.; Yuzawa, N.; Chantana, J.; Minemoto, T.; Nose, Y. Solar Cells Using Bulk Crystals of Rare Metal-Free Compound Semiconductor ZnSnP<sub>2</sub>. *Phys. Status Solidi A* **2017**, *214*, 1600650.
- (16) Nakatani, K.; Minemura, T.; Miyauchi, K.; Fukabori, K.; Nakanishi, H.; Sugiyama, M.; Shirakata, S. Photoluminescence Property of ZnSnP<sub>2</sub> by Solution Growth and Normal Freezing Methods. *Jpn. J. Appl. Phys.* **2008**, *47*, 5342–5344.
- (17) Shockley, W.; Queisser, H. J. Detailed Balance Limit of Efficiency of PN Junction Solar Cells. *J. Appl. Phys.* **1961**, *32*, 510-519.
- (18) Yokoyama, T.; Oba, F.; Seko, A.; Hayashi, H.; Nose, Y.; Tanaka, I. Theoretical Photovoltaic Conversion Efficiencies of ZnSnP<sub>2</sub>, CdSnP<sub>2</sub>, and Zn<sub>1-x</sub>Cd<sub>x</sub>SnP<sub>2</sub> Alloys. *Appl. Phys. Express* **2013**, *6*, 61201.
- (19) Shin, H. Y.; Ajmera, P. K. Characterization of Vacuum Grown Thin Films of ZnSnP<sub>2</sub>. *Mater. Lett.* **1987**, *5*, 211-214.
- (20) Minoura, S.; Kadera, K.; Maekawa, T.; Miyazaki, K.; Niki, S.; Fujiwara, H. Dielectric function of Cu(In,Ga)Se<sub>2</sub>-Based Polycrystalline Materials. *J. Appl. Phys.* **2013**, *113*, 63505.
- (21) Yuzawa, N.; Chantana, J.; Nakatsuka, S.; Nose, Y.; Minemoto, T. ZnSnP<sub>2</sub> thin-

- film solar cell prepared by phosphidation method under optimized Zn/Sn atomic ratio of its absorbing layer. *Curr. Appl. Phys.* **2017**, *17*, 557–564.
- (22) Nakatsuka, S.; Akari, S.; Chantana, J.; Minemoto, T.; Nose, Y. Impact of Heterointerfaces in Solar Cells Using ZnSnP<sub>2</sub> Bulk Crystals. *ACS Appl. Mater. Interfaces* **2017**, *9*, 33827–33832.
- (23) Akari, S.; Chantana, J.; Nakatsuka, S.; Nose, Y.; Minemoto, T. ZnSnP<sub>2</sub> Solar Cell with (Cd,Zn)S Buffer Layer: Analysis of Recombination Rates. *Sol. Energy Mater. Sol. Cells* **2018**, *174*, 412–417.
- (24) Nakatsuka, S.; Nose, Y.; Shirai, Y. Band Offset at the Heterojunction Interfaces of CdS/ZnSnP<sub>2</sub>, ZnS/ZnSnP<sub>2</sub>, and In<sub>2</sub>S<sub>3</sub>/ZnSnP<sub>2</sub>. *J. Appl. Phys.* **2016**, *119*, 193107.
- (25) Shay, J. L.; Wernick, J. H. *Chalcopyrite Semiconductors: Growth, Electronic Properties, and Applications*; Pergamon Press: Oxford, 1975.
- (26) Kumagai, Y.; Choi, M.; Nose, Y.; Oba, F. *Phys. Rev. B* First-principles study of point defects in chalcopyrite ZnSnP<sub>2</sub>. *Condens. Matter Mater. Phys.* **2014**, *90*, 1-12.
- (27) Higashino, T.; Nose, Y.; Toyoura, K.; Uda, T. *Bulk Crystal Growth of Chalcopyrite Semiconductors of the Zn-Cd-Sn-P System Based on the Phase Diagram*. MRS Fall Meeting, Boston, USA, Nov 28–Dec 2, 2011.

- (28) Nakatsuka, S.; Nose, Y.; Uda, T. Fabrication of ZnSnP<sub>2</sub> thin films by phosphidation. *Thin Solid Films* **2015**, *589*, 66-71.
- (29) Yokokawa, H. Generalized Chemical Potential Diagram and Its Applications to Chemical Reactions at Interfaces Between Dissimilar Materials. *J. Phase Equilibria* **1999**, *20*, 258-287.
- (30) Barin, I. *Thermochemical Data of Pure Substances, third ed.*; VCH Verlagsgesellschaft GmbH: Weinheim, 1995.
- (31) Sirota, N. N., Antyukhov, A. M., Smolyarenko, E. M. Investigation into Thermodynamic Properties of Cd-P System Compound by Electromotive Forces Method. *Dokl. Akad. Nauk SSSR* **1974**, *219*, 397.
- (32) Smolyarenko, E. M. Yakimovich, V. N. Thermodynamics of Formation of ZnSnP<sub>2</sub> and CdSnP<sub>2</sub>. *Izv. Akad. Nauk SSSR, Neorg. Mater* **1981**, *17*, 132-134.
- (33) Wagner, R. S.; Ellis, W. C. Vapor-Liquid-Solid Mechanism of Single Crystal Growth. *Appl. Phys. Lett.* **1964**, *4*, 89-90.

## ■ Figure captions

Figure 1. XRD profiles of Cd-Sn thin films before and after phosphidation for 30 min at various temperatures.

Figure 2. SEM images of Cd-Sn thin films before and after phosphidation for 30 min at various temperatures.

Figure 3. Cross-sectional SEM images of Cd-Sn thin films (a) before and (b) after phosphidation at 350 °C.

Figure 4. XRD profiles of Cd-Sn thin films before and after phosphidation at 300 °C.

“Discontinued” indicates the sample discontinued on the way heating up to 300 °C.

Figure 5. SEM images of thin films (a) before phosphidation, (b) discontinued during heating up, and after phosphidation at 300 °C (c) 5 min and (d) 30 min.

Figure 6. Chemical potential diagrams of (a) Cd-Sn-P system at 300 °C and (b) Zn-Sn-P system at 450 °C.

## ■ Figures

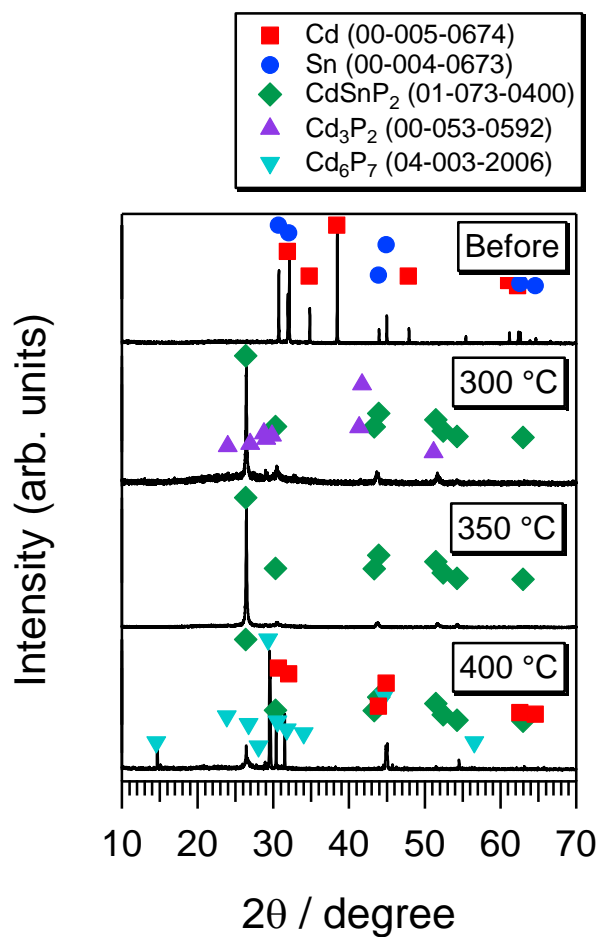


Fig. 1. XRD profiles of Cd-Sn thin films before and after phosphidation for 30 min at various temperatures.

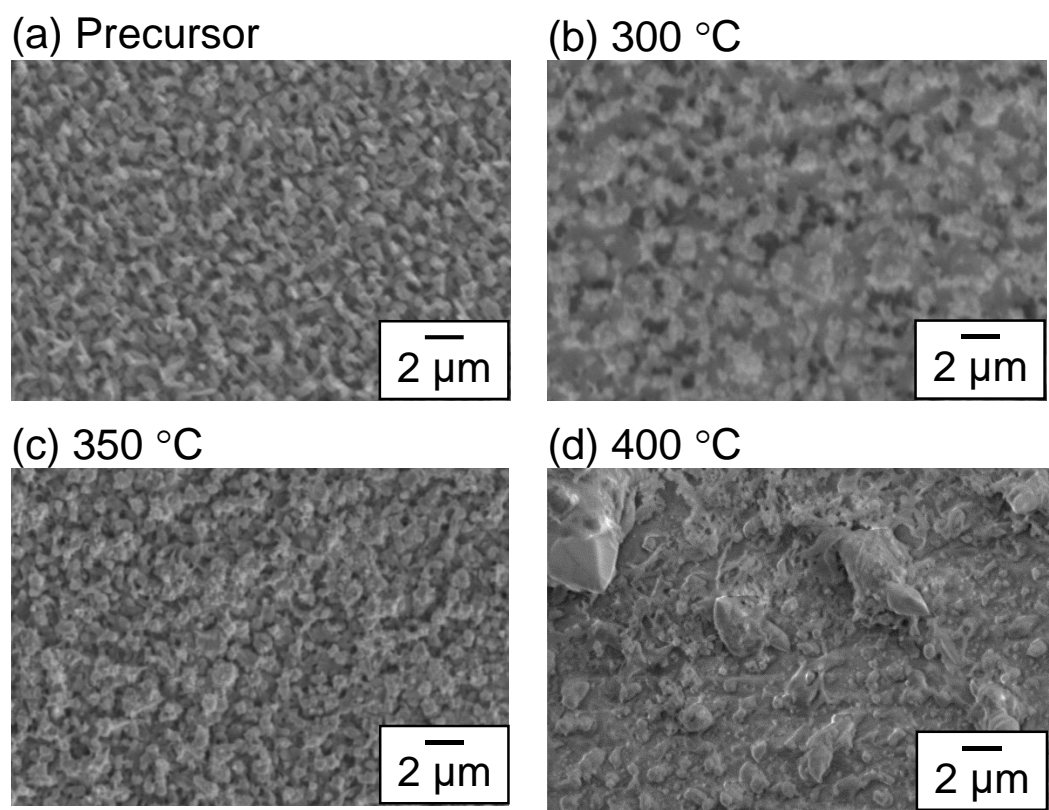


Fig. 2. SEM images of Cd-Sn thin films before and after phosphidation for 30 min at various temperatures.

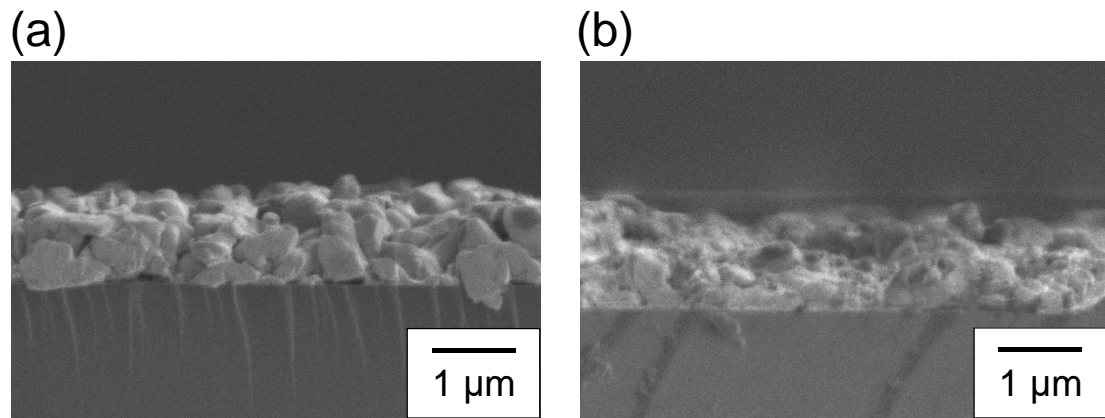


Fig. 3. Cross-sectional SEM images of Cd-Sn thin films (a) before and (b) after phosphidation at 350 °C.



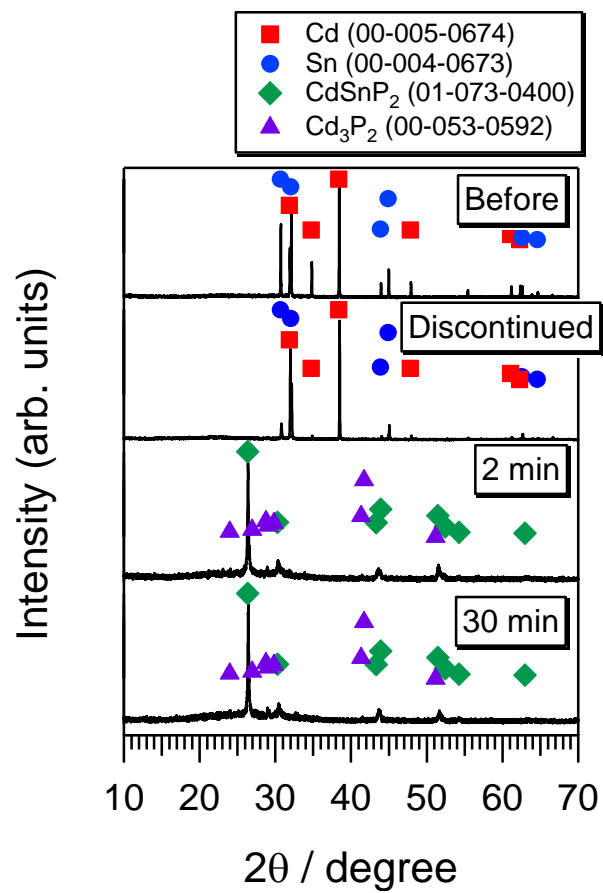


Fig. 4. XRD profiles of Cd-Sn thin films before and after phosphidation at 300 °C.

“Discontinued” indicates the sample discontinued on the way heating up to 300 °C.

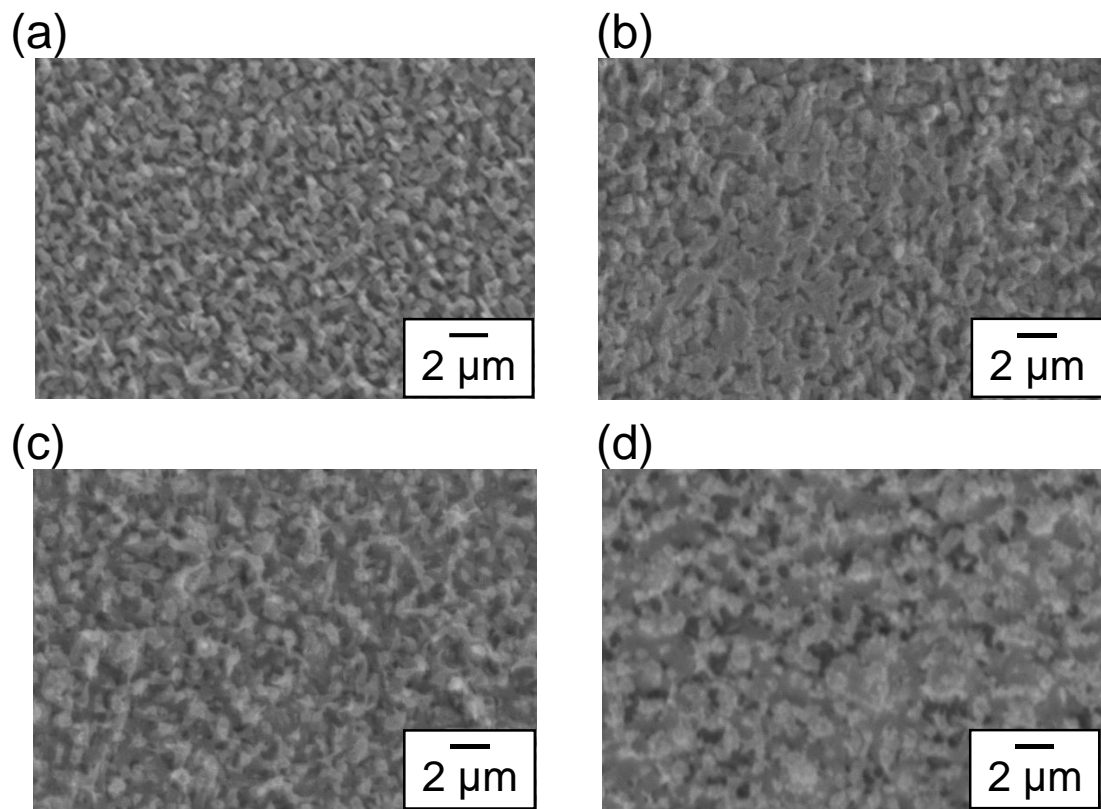
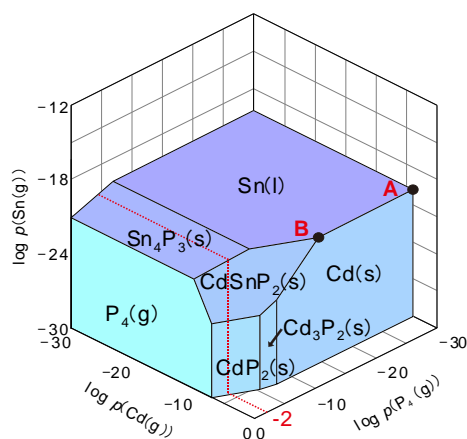


Fig. 5. SEM images of thin films (a) before phosphidation, (b) discontinued during heating up, and after phosphidation at 300 °C (c) 5 min and (d) 30 min.

(a)



(b)

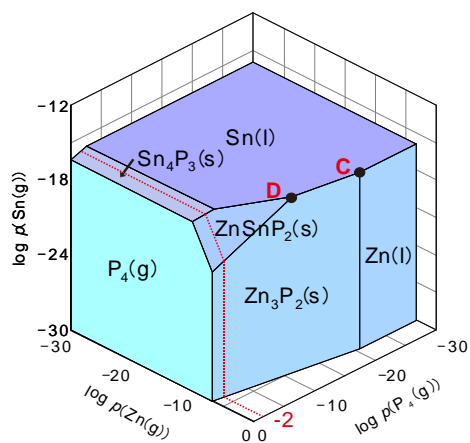


Fig. 6. Chemical potential diagrams of (a) Cd-Sn-P system at 300 °C and (b) Zn-Sn-P system at 450 °C.

## ■ Table of Contents (TOC) Image

